Structural Features of the UCCG and UGCG Tetraloops in Very Short Hairpins As Evidenced by Optical Spectroscopy†

M. Abdelkafi,‡ N. Leulliot,‡ V. Baumruk,§ L. Bednárová,|| P. Y. Turpin,‡ A. Namane,⊥ C. Gouyette,⊥ T. Huynh-Dinh,⊥ and M. Ghomi*,‡

Laboratoire de Physicochimie Biomoléculaire et Cellulaire, URA CNRS 2056, Université Pierre et Marie Curie, Case 138, 4 Place Jussieu, 75252 Paris Cedex 05, France, Institute of Physics, Charles University, Ke Karlovu 5, 12116 Prague 2, Czech Republic, Institute of Organic Chemistry and Biochemistry, Czech Academy of Sciences, Flemingovo nám. 2, 16610 Prague 6, Czech Republic, and Unité de Chimie Organique, URA CNRS 487, Institut Pasteur, 28 rue du Docteur Roux, 75724 Paris Cedex 15, France

Received January 5, 1998; Revised Manuscript Received February 19, 1998

ABSTRACT: Structures of the UCCG and UGCG tetraloops formed in octamer ribonucleotidic hairpin sequences, i.e., 5′-r[GC(UCCG)GC]-3′ and 5′-r[GC(UGCG)GC]-3′, have been studied in aqueous solution by methods of optical spectroscopy. UV absorption melting profiles of these short hairpins, containing only two closing GC base pairs in the stem, are consistent with a monophasic, completely reversible order-to-disorder transition and clearly confirm their unusual structural stability (with $T_m \cong 50$ °C). To establish structural characteristics of these tetraloops, Raman and FTIR spectroscopies have been used and vibrational conformation markers arising from the phosphate backbone and various nucleosides have been analyzed. They have been assigned on the basis of known unambiguous vibrational markers established for DNA and RNA chains. Surprisingly, they are easily transferable to short oligonucleotidic sequences. Intensities and wavenumbers of these conformation markers have been monitored in the 0−70 °C temperature range, i.e., in going from an ordered to a disordered structure. The main structural features of the UCCG and UGCG tetraloops are similar to those previously found in the UUCG and UACG tetraloops by means of NMR and vibrational spectroscopies, except those of the second nucleosides of the tetraloops (rC and rG, respectively) which adopt a 3′-endo/anti rather than a 2′-endo/anti conformation.

UNCG sequences (N = U, A, C, G) are considered as elementary tracks able to form tetraloop hairpins which can serve as nucleation sites for RNA folding (*1*−*5*). These tetraloops create, through specific intramolecular (hydrogen bonds and van der Waals and Coulombic interactions) and intermolecular (RNA−solvent) interactions, particular spatial configurations that surprisingly increase their structural and thermodynamic stability.

Several investigations made by means of various physical techniques have been devoted to the understanding of the structural features of the UUCG and UACG tetraloops. One can mention here the thermodynamical parameters obtained from UV absorption melting profiles of the UUCG (*6*−*13*) and the UACG (*9*, *10*, *12*, *13*) tetraloops. High melting temperatures of the UUCG and UACG tetraloops have first been evidenced in aqueous phase for hairpins formed in the 13-mer r[UGAGC(UUCG)GCUC] (*6*), the 12-mer r[GGAC-(UUCG)GUCC] (*7*, *8*), and the 12-mer r(GGAC(UACG)-GUCC) (*9*, *10*). Molinaro and Tinoco (*11*) examined whether this unusual structural stability has to be considered as an inherent feature of the UUCG tetraloop or also depends on the nature and the length of the closing base-pair sequence in the hairpin stems. Their results, mainly based on studies of synthetic oligoribonucleotides of different lengths (6−12 residues) including the UUCG sequence in their central part, showed the following features: the stem should contain at least two GC base pairs to form a stable hairpin with a sigmoidal melting profile characteristic for an order-to-disorder transition. Experiments on hairpins having only one closing GC base pair show a rather flat melting profile without any unambiguous T_m. Moreover, CG closing base pairs provide more stable hairpins than GC ones. It has also been shown (*11*) that, by replacing G by A at the ultimate 3′ position of the UUCG tetraloop, the hairpin melting temperature is lowered by about 25 °C. Recently, the melting profiles of very short hairpins formed in the octamers r[GC(UUCG)GC] and r[GC(UACG)GC] (*12*, *13*) also revealed high T_m values, i.e., 54 and 51 °C, respectively.

High-resolution NMR data allowed a very particular internal structure of the UUCG (*6*−*8*) and UACG (*13*, *14*) tetraloop hairpins to be resolved: (i) The terminal guanine base of the loop has a syn orientation vs sugar. (ii) The middle two nucleosides in both tetraloops possess 2′-endo

† This work was partly supported by the Grant Agency of the Charles University (Project 9/97). M.A. was supported by a fellowship from the Institut Aulnaysien de Développement Economique (Aulnay-sous-Bois). N.L. was supported by a study grant from the MENESR. V.B. would like to thank MENESR and French Ministry of Foreign Affairs for a senior scientist fellowship.

* To whom all correspondence should be addressed. Fax: 33 (1) 44277560. E-mail: ghomi@lpbc.jussieu.fr.

‡ Université Pierre et Marie Curie.

§ Charles University.

|| Czech Academy of Sciences.

⊥ Institut Pasteur.

S0006-2960(98)00011-7 CCC: $15.00
Published on Web 05/02/1998

sugar puckers (S-type). (iii) Possible base-pairing contacts exist between the ultimate U and G bases of the loop. Two different models have been proposed for this base pair: in the first, the base pair exists as a reverse-wobble type (*7, 8*); in the second, the O2 atom of the uracil and the 2′-OH of the rG sugar pucker are involved in the H-bond network (*15*). However, whatever the nature of the UG base pair is, the tetraloop should be considered as a "diloop", containing only two unpaired bases, i.e., the central UC and AC bases in UUCG an UACG tetraloops, respectively. (iv) The stem in these hairpins adopts a standard A-form double-helical conformation.

Furthermore, as evidenced by NMR data in the UUCG and UACG tetraloops, the second base (U and A, respectively) is oriented outward from the loop (*7, 8, 13*). Consequently, it interacts less tightly with the nucleotides involved in the loop. Distance-constrained molecular modeling based on NMR data related to the UUCG 12-mer also revealed that the C base in the third position is somehow stacked to the first U base in the loop, thus increasing the structural stability of the hairpin (*7, 8*). Simulation of quantitative NOESY volumes showed that the UACG octamer adopts a very rigid and compact structure which is well represented by an average order parameter $S^2 = 0.9$ (*13*).

Vibrational conformation markers, assigned and analyzed in both the UUCG (*12*) and UACG (*13*) tetraloops, support the structural features evidenced by NMR. The aim of the present work is to analyze the other two tetraloops of the UNCG family, i.e., UCCG and UGCG, for which no NMR data are yet available, by studying UV absorption melting profiles as well as vibrational markers. Indeed, vibrational markers can be successfully used to monitor the tetraloop conformation within the hairpins only if the number of residues included in the stem is not too high as compared to that of the loop: for this reason, we limited the present study to hairpins containing only two GC base pairs in their stem.

MATERIALS AND METHODS

Chemical synthesis of the UNCG octamers has been described in detail recently (*13*). Following this procedure, approximately 3.5 mg of the 5′-r[GC(UCCG)GC]-3′ and 5′-r[GC(UGCG)GC]-3′ octaribonucleotides has been obtained for recording optical spectra. The octamer solutions were prepared in a 10 mM phosphate buffer, pH 7 (pD 7), freed of possible divalent ions by the addition of EDTA (0.1 mM). No salt was added to the buffer. Thus the counterions stabilizing the phosphate charges were only those present in the lyophilized sample prepared after chemical synthesis (1 Na^+ per phosphate group). The final concentrations of octamers in aqueous solutions were 40 μM and 1 mM for UV absorption and 10 mM for FTIR and Raman spectroscopy.

Experimental details concerning measurement of UV absorption, FTIR, and Raman spectra of the oligoribonucleotides have been reported in our previous papers (*13, 16, 17*). Melting profiles have been obtained by monitoring the absorbance at 240 nm in the 10−70 °C temperature range with a 1 °C step for two different sample concentrations (40 μM and 1 mM). A two-states model allowed the thermodynamical parameters T_m, $\Delta H°$, and $\Delta S°$ (melting temperature and enthalpy and entropy variations, respectively) to be determined in going from an ordered to a disordered conformation (*16*). Raman spectra were recorded by exciting the samples in a microcell (10 μL inner volume) (*18*) with the 488- or 514.5-nm lines of an argon ion laser (150 mW of radiant power at the sample). The spectral slit width was 5 cm^{-1}. For recording FTIR, the samples were placed in a demountable cell consisting of a pair of ZnSe windows separated by a 15 μm Teflon spacer. The spectral resolution was 4 cm^{-1}.

The reversibility of the structural transitions (hairpin to disordered and/or disordered to hairpin) has been verified by gradually heating the samples from 0 °C to the highest temperature limit (≈70 °C) and cooling to 20 °C. Optical spectra (UV absorption, FTIR, and Raman scattering) taken at 20 °C before and after this thermal annealing were exactly the same. The temperature gradient across the sample cell was less than 0.5 °C.

RESULTS AND DISCUSSION

Thermodynamic Parameters. Concentration-independent melting profiles of the UCCG and UGCG hairpins (Figure 1) are consistent with a transition from ordered (hairpin) to disordered (random chain) structure. Similar profiles have been observed for the other two UNCG tetraloops, i.e., UUCG and UACG (*13*). Thermodynamic parameters of all the UNCG (N = U, A, C, G) hairpins are summarized in Table 1. The T_m values of the four UNCG hairpins (formed in the octamers) are located within the 48.5−54 °C temperature range; in decreasing order, UUCG > UACG > UCCG > UGCG (Table 1).

In fact, the equilibrium between intramolecular hairpin and intermolecular duplex conformations strongly depends on the octamer concentration in the aqueous phase. To get duplexes as the major population, the concentration has to be about 1 order of magnitude higher than that routinely used in NMR and vibrational spectroscopy (ca. 15 mM). Of course, the salt concentration also plays a major role in this kind of intermolecular binding. Recent studies on r[GGAC(UUCG)GUCC] (*19*) have shown that, in the low-concentration range, the formation of intramolecular hairpin is favored, whereas the crystal growth from the mother liquor of this dodecamer, leading to duplexes as confirmed by X-ray diffraction patterns, was only possible at molecular and salt (NaCl) concentrations of 180 mM and 2.5 M, respectively.

Vibrational Markers. (A) Order-to-Disorder Transition: Breakdown of the Intramolecular H-Bond Network upon Melting. In Figures 2 and 3 are presented the Raman spectra obtained from the UCCG and UGCG teraloops, respectively, in the 0−70 °C temperature range. In the 1750−1100 cm^{-1} spectral region and for temperatures higher than T_m, Raman spectra of the octamers are changed dramatically and closely resemble the reconstituted spectral profiles obtained as a sum of the Raman spectra of monomeric constituents (not shown). The observed wavenumbers (at 0 °C) of the most prominent Raman markers of the octamers containing the UCCG and UGCG tetraloops, as well as their assignments, are summarized in Table 2.

The breakdown of the hydrogen bond network can be observed in the 1750−1650 cm^{-1} spectral region. For both octamers, spectral changes in the 0−70 °C range clearly show

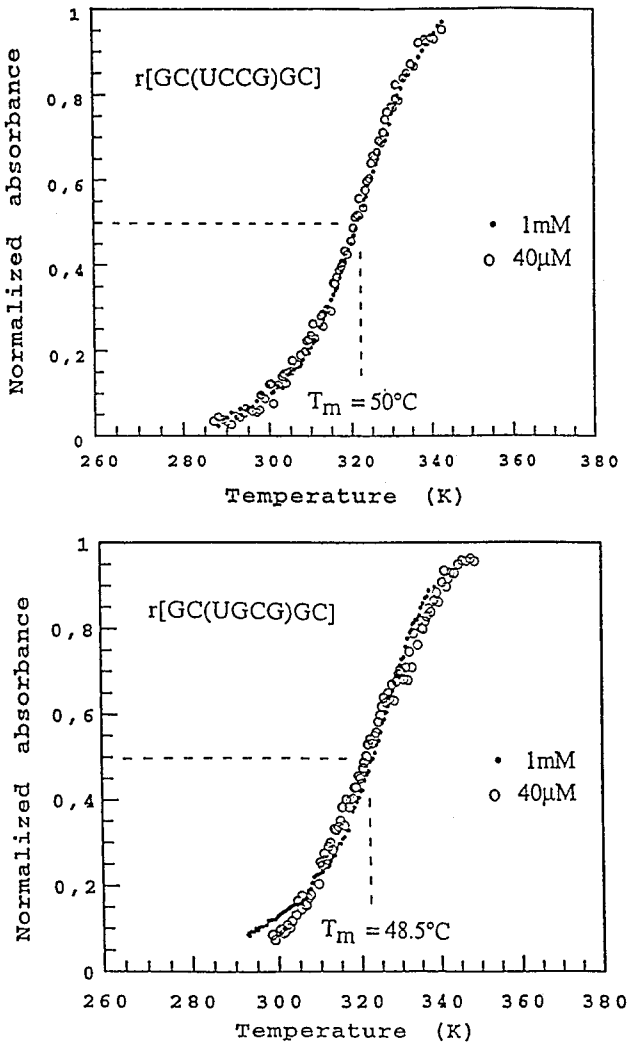

FIGURE 1: UV absorption melting profiles of the r[GC(UCCG)-GC] and r[GC(UGCG)GC] hairpins in aqueous solution at two octamer concentrations. To draw these curves, the normalized optical density (NOD) of the absorption band at 240 nm has been followed as a function of the temperature. T_m corresponds to equal populations of ordered and disordered conformers in solution (NOD = 0.5). See in Table 2 the thermodynamic parameters for all of the UNCG hairpins.

Table 1: Thermodynamic Parameters of UNCG Octamers (N = U, A, C, G) Determined from Their Melting Profiles

	T_m (°C)	$\Delta H°$ (kcal/mol)	$\Delta S°$ (cal/mol K)
r[GC(UUCG)GC][a,b]	54.0 ± 0.3	−25.5 ± 0.5	−78 ± 2
r[GC(UACG)GC][a]	51.0 ± 0.3	−26.3 ± 0.5	−81 ± 3
r[GC(UCCG)GC][c]	50.0 ± 0.5	−23.6 ± 0.5	−73 ± 3
r[GC(UGCG)GC][c]	48.5 ± 0.5	−22.5 ± 0.7	−70 ± 3

[a] From refs *12* and *13*. [b] The T_m value of the same octamer reported in ref *11* is 54.9 °C. [c] This work. See also Figure 1 for the melting profiles of the UCCG and UGCG tetraloop hairpins.

the gradual disappearance of the band at 1708 cm^{-1} (mainly assignable to a C═O stretching mode) (*20*) as well as the disappearance of a shoulder observed around 1670 cm^{-1} (double-bond stretching of the bases). At high temperature the Raman bands of this group become less structured and only a broad band is observed in this region.

On the other hand, FTIR spectra of the octamers observed in the 1710−1540 cm^{-1} spectral region in D_2O and in the 0−70 °C temperature range also provide a wealth of

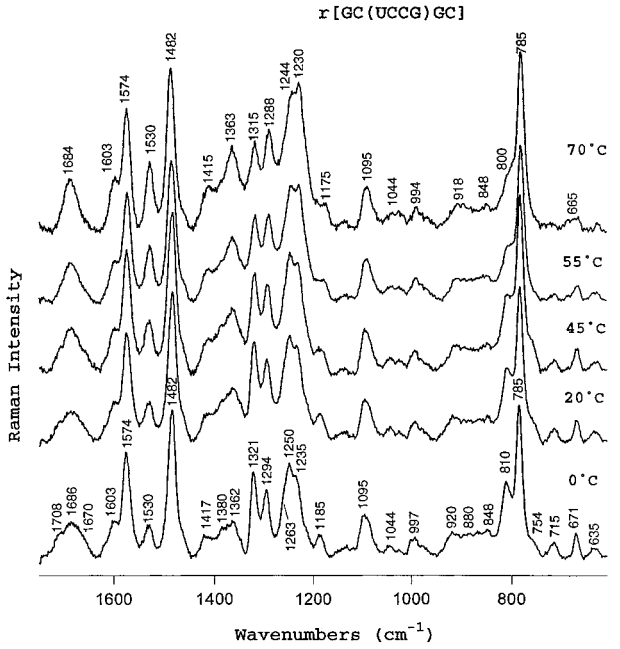

FIGURE 2: Evolution of the Raman spectra of the r[GC(UCCG)-GC] octamer observed in H_2O buffer as a function of temperature (0−68 °C) in the 1750−600 cm^{-1} spectral region. Excitation wavelength: λ_{exc} = 514.5 nm. Spectra were normalized on the $\nu_s(PO_2^-)$ band at ca. 1095 cm^{-1} as an internal standard.

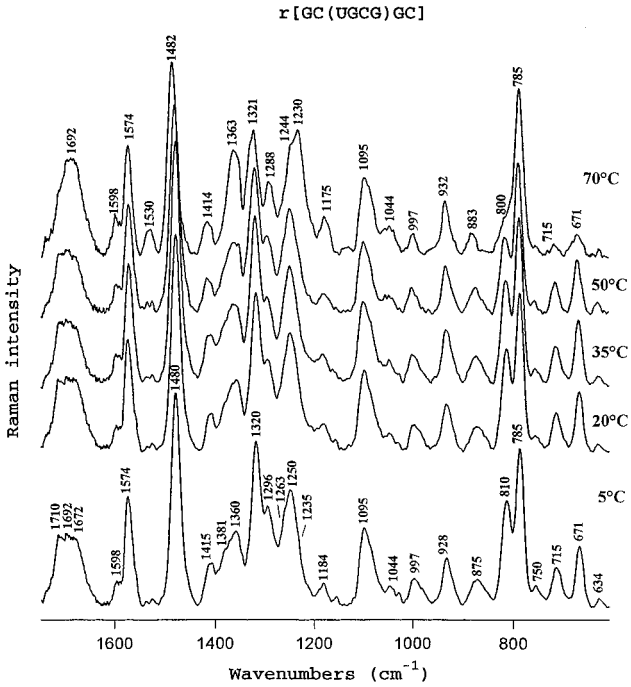

FIGURE 3: Evolution of the Raman spectra of the r[GC(UGCG)-GC] octamer observed in H_2O buffer as a function of the temperature (0−68 °C) in the 1750−600 cm^{-1} spectral region. Excitation wavelength: λ_{exc} = 514.5 nm. Spectra were normalized on the $\nu_s(PO_2^-)$ band at ca. 1095 cm^{-1} as an internal standard.

information on the interbase hydrogen bond network. Figure 4A displays this spectral region for the UCCG tetraloop. The most prominent temperature effect is the gradual disappearance of the intense band at 1683 cm^{-1}, assigned to C═O stretching modes (*21*) mainly arising from the guanine bases involved in the GC and UG base pairs in the stem and in the loop, respectively. This band is downshifted and superimposed with an intense IR band at 1658 cm^{-1},

Table 2: Wavenumbers (cm^{-1}) and Assignments of the Most Prominent Raman Marker Bands Observed at 0 °C in r[GC(UCCG)GC] and r[GC(UGCG)GC] Hairpins

r[GC(UCCG)GC][a]	r[GC(UGCG)GC][a]	assignment
1708 (sh)	1710 (m, br)	base C═O; stem
1686 (m, br)	1692 (m, br)	base C═O; stem and loop
1670 (sh)	1672 (m, br)	base double-bond; stem and loop
1603 (sh)	1598 (sh)	r(C); 3′-endo/anti; stem
1574 (vs)	1574 (vs)	r(G); stem and loop
1530 (m)	1525 (w)	r(C); 3′-endo/anti; stem
1482 (vs)	1480 (vs)	r(G); stem and loop
1417 (m, br)	1415 (m, br)	r(G); stem and loop
1380 (sh)	1381 (sh)	r(G); 3′-endo/anti; stem
1362 (m)	1360 (m)	r(G); 3′-endo/syn; loop
1321 (vs)	1320 (s)	r(G); 3′-endo/syn; loop and 3′-endo/anti; stem
1294 (s)	1296 (m)	r(C); 3′-endo/anti; stem and loop
1263 (sh)	1263 (sh)	r(C); 2′-endo/anti; loop
1250 (vs)	1250 (s)	r(C); 3′-endo/anti; loop and stem
1235 (sh)	1235 (sh)	r(U); loop
1185 (m)	1184 (m)	r(G); 3′-endo/syn; loop
1095 (m)	1095 (m)	PO_2^- symmetric stretch
1044 (w)	1044 (w)	backbone, ribose
997 (w)	997 (w)	backbone
	928 (m)	backbone
920 (m)	916 (sh)	backbone
880 (w)	875 (w)	backbone
848 (w)		backbone
810 (m)	810 (m)	O−P−O symmetric stretch (A marker)
785 (vs)	785 (vs)	r(C); stem and loop; r(U); loop
754 (sh)	750 (sh)	backbone; loop
715 (w)	715 (w)	backbone; stem (A marker)
671 (w)	671 (w)	r(G); 3′-endo/anti; loop and stem
635 (w)	634 (w)	r(G); 3′-endo/syn; loop

[a] Abbreviations: vs, very strong; s, strong; m, medium; w, weak; vw, very weak; br, broad; sh, shoulder.

temperature independent and arising from the base double-bond stretchings. It is worth noting that the 5′-rGMP FTIR spectrum in D_2O provides a very intense band at 1664 cm^{-1} (spectrum not shown). In the same spectral range, the behavior of the 1576−1564 cm^{-1} doublet, mainly arising from the G-residue double-bond stretching vibrations, should be emphasized: the intensity ratio of these two bands is considerably changed with increasing temperature (Figure 4A).

(B) Phosphate Backbone Markers. In the low-wavenumber region of the Raman spectra, the presence of the intense band around 810 cm^{-1} has been previously used as an A-form marker of ordered RNA helixes (*22*−*24*). In the Raman spectra of the UCCG and UGCG octamers (Figures 2 and 3), and also in those of the UUCG and UACG octamers (*12*, *13*), an intense band at 810 cm^{-1} can be observed, which vanishes at high temperature. It is assigned to O−P−O symmetric stretching vibrations, coupled with 3′-endo sugar vibrational motions (*25*) for the phosphate groups included in the stem. However, a possible contribution of the phosphate groups of the loop flanked by N-type sugars should also be taken into consideration.

To get more information about the structural irregularities of the phosphate backbone chain, the 1150−800 cm^{-1} spectral regions have been analyzed in the FTIR spectra taken

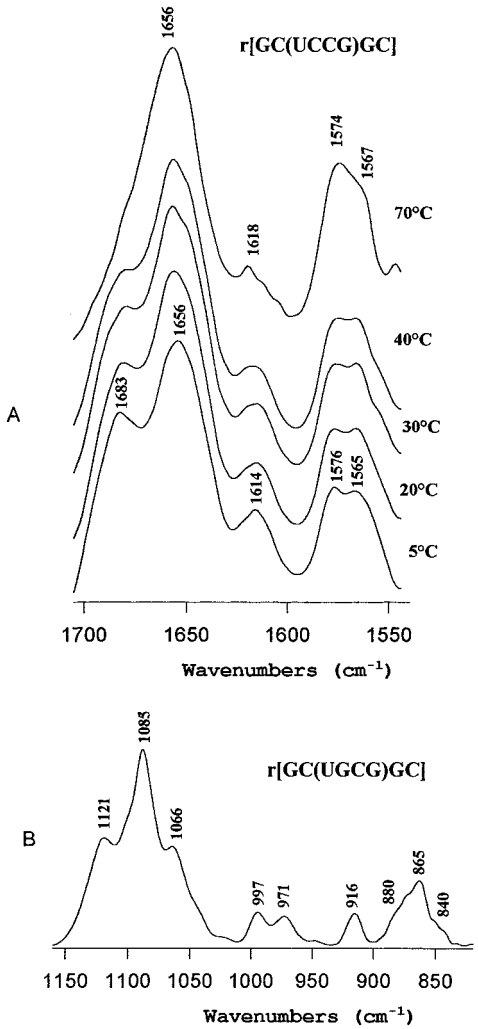

FIGURE 4: (A) FTIR spectra of the r[GC(UCCG)GC] octamer observed in D_2O buffer as a function of the temperature in the 1710−1540 cm^{-1} spectral region. The various spectra of each octamer were normalized on the $\nu_s(PO_2^-)$ band at ca. 1085 cm^{-1} as an internal standard. (B) FTIR spectrum of the r[GC(UGCG)GC] octamer observed in H_2O buffer in the 1150−800 cm^{-1} spectral region.

in H_2O solutions. Figures 4B presents this spectral region for the UGCG hairpin. Regardless of the PO_2^- symmetric bond-stretching mode at 1085 cm^{-1}, the characteristic IR bands corresponding to N-type sugar pucker vibrations can clearly be observed at 1121, 1066, 997, 971, 916, 880, and 865 cm^{-1} (*21*, *26*), the latter being coupled with the O−P−O antisymmetric bond-stretching vibration (*25*, *27*). Some of these bands can also be observed, more and less resolved, in the 950−860 cm^{-1} spectral region of the various Raman spectra (Figures 2 and 3; see also refs *12* and *13*). The only IR marker assignable to S-type sugar pucker is the low-intensity band located around 840 cm^{-1} (Figure 4B), which also appears as a very weak band in the Raman spectra around 850 cm^{-1} (Figures 2 and 3). Very close spectral profiles were obtained in this domain for the other sequences. On the basis of these observations one can conclude that all of these hairpins mainly include N-type sugar puckers in their structure. However, the existence of S-type sugars cannot be completely ruled out, but their number should remain very low.

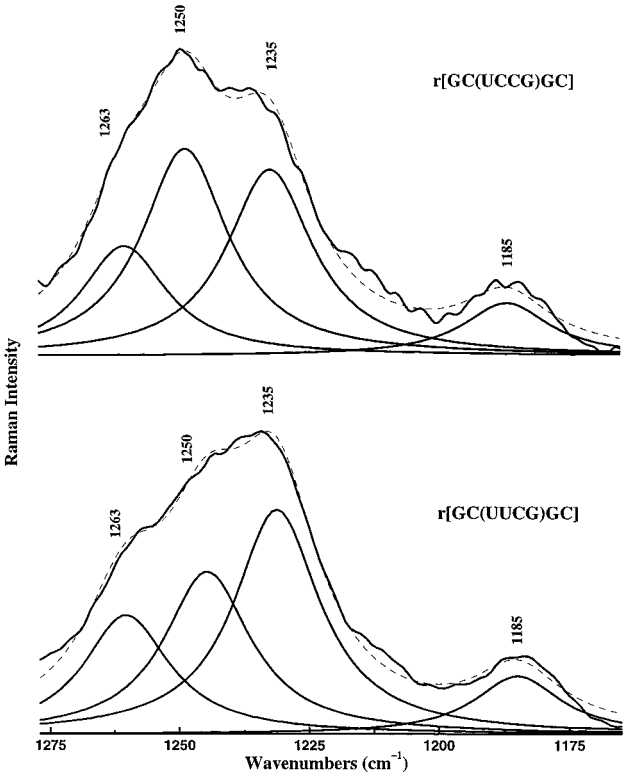

FIGURE 5: Tentative band decomposition of Raman spectra of the UCCG and UUCG hairpins observed in H_2O buffer at 0 °C in the 1275−1160 cm^{-1} spectral region. Excitation wavelength: λ_{exc} = 514.5 nm. Dashed curves correspond to the sum of the decomposed bands.

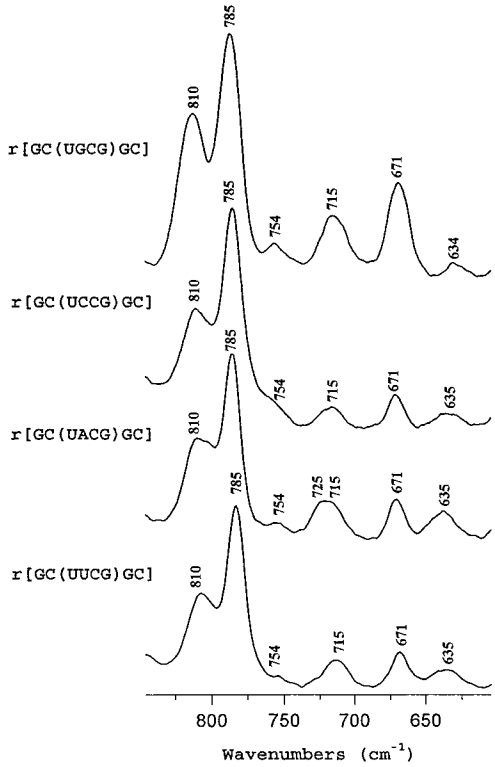

FIGURE 6: Comparison of the Raman spectra of the various UNCG hairpins (N = U, A, C, G) observed in H_2O buffer at 0 °C, in the 850−600 cm^{-1} spectral region. Excitation wavelength: λ_{exc} = 514.5 nm.

(C) Conformational Markers of the Nucleosides Involved in the Stem and in the Loop. Let us now discuss the Raman bands observed in two important spectral regions, i.e., 1400−1150 and 750−600 cm^{-1}, corresponding to base-residue vibrational modes sensitive to the syn or anti orientations of the base vs sugar and to the S- and N-type sugar puckers (Figures 2 and 3).

Undoubtedly, the most characteristic Raman band of the first spectral region is that observed at 1321 cm^{-1}, assigned to rG residues. In the Raman spectra of the UCCG and UGCG tetraloops, the intensity of this band decreases drastically on an increase of the temperature (Figures 2 and 3). The same temperature dependence of this Raman marker has also been observed in the case of the UUCG and UACG tetraloops (*12, 13*). Indeed, the intensity of this mode strongly depends on the orientation of the G base with respect to the sugar. This has been established by Raman measurements of DNA or RNA double helixes containing GC base pairs, undergoing B−Z (*28*−*31*) or A−Z (*31*) transitions, respectively. The G base is known to have an anti orientation in both A-RNA and B-DNA helixes, whereas it adopts a syn orientation in Z-DNA and Z-RNA helixes. Under Z forms, the intensities of the dG or rG 1321 cm^{-1} Raman markers are drastically increased. Thus, the behavior of the 1321 cm^{-1} Raman band as a function of temperature clearly shows that, in all the structured UNCG hairpins (N = U, A, C, G), the ultimate G base has a syn orientation.

Another G residue syn orientation marker is the low-intensity Raman band at 1185 cm^{-1} (*31*) which is gradually downshifted to 1175 cm^{-1} by increasing the temperature. Moreover, two Raman bands around 1380 and 1360 cm^{-1} (at low temperature) can also be taken as marker bands for the rG residues, located in the stem (3′-endo/anti) or in the tetraloop (3′-endo/syn), respectively. This assignment is also based on Raman studies of polyribonucleotides in A-form (*31, 32*) and Z-form (*31*), showing Raman markers at 1388 and 1355 cm^{-1}, respectively. In the UCCG and UGCG octamers (Figures 2 and 3), as well as in the UUCG and UACG tetraloops (*12, 13*), these two Raman bands merge at high temperature, giving rise to a broad, intense band around 1363 cm^{-1}.

In the second spectral region (Figures 2 and 3), the Raman band observed around 635 cm^{-1} at low temperature is also a marker of the 3′-endo/syn orientation of the rG residue in the loop. Its wavenumber value corresponds well to that observed in Z forms of RNAs (*30, 31*).

The behavior of all of the rG residue markers mentioned above, especially those related to 3′-endo/syn conformation of the last nucleoside in the loop, is consistent with a gradual opening of UNCG tetraloops as a function of the temperature, consequently leading to the decrease of the hairpin and the increase of the random chain populations.

(D) N-Type Sugar Pucker of the rC and rG Residues Located at the Second Position of the UCCG and UGCG Tetraloops. Let us now further discuss the sugar pucker conformations of the residues involved in the UCCG and UGCG loops. As stated above, phosphate backbone markers show that there probably exists 2′-endo sugar puckers in the loop, their number remaining rather low.

In the Raman spectra of all the UNCG tetraloops, the behavior of the 1263 cm^{-1} Raman shoulder arising from rC residues should be emphasized (Figures 2 and 3 and (*13*)). This shoulder is located at the high-wavenumber limb of the

medium-intensity Raman band at 1250 cm^{-1} assigned to 3′-endo/anti rC residues involved in the stem. The assignment of the 1263 cm^{-1} mode is based, on one hand, on the analysis of B-form and Z-form DNA (*29*), both containing 2′-endo/anti dC residues and showing an intense Raman band around 1265 cm^{-1}, and on the other, on Z-form RNAs such as poly(rG-rC) (*31*) and r$(CG)_3$ (*30*), showing a 2′-endo/anti rC Raman band at 1264 cm^{-1}.

To estimate as accurately as possible maxima and intensities of the rC residue conformational markers (1263 and 1250 cm^{-1}), a tentative band decomposition in the 1275−1160 cm^{-1} spectral region is presented in Figure 5 for UCCG and UUCG tetraloops. This comparison shows that (i) the intensity of the 1235 cm^{-1} rU marker is increased in the case of the UUCG tetraloop which contains an additional uracil in the loop, (ii) the intensity of the 1263 cm^{-1} band remains unchanged in both cases, and (iii) the intensity of the 1250 cm^{-1} band increases in the UCCG hairpin, which includes an additional rC residue at the second position of the loop. This indicates that the *second rC residue* in the UCCG tetraloop has a 3′-endo/anti conformation and that the *third rC residue*, which is common to all the UNCG sequences, adopts a 2′-endo/anti conformation.

The conformation of the sugar pucker involved in the second rG residue conformation of the UGCG tetraloop can be analyzed by means of the 671 cm^{-1} Raman band whose position is unchanged over all of the tetraloops (Figure 6). This band is assigned to a 3′-endo/anti rG configuration, as shown in the Raman spectra of the A-form of poly(rG-rC) (*31*) and r$(CG)_3$ (*30*). If the rG residue were in 2′-endo/anti conformation, the corresponding wavenumber of this marker would be around 685 cm^{-1}, as in B-form DNA (*28*, *29*) and in 5′-rGMP (Raman spectrum not shown). This means that the second rG residue configuration in the UGCG tetraloop also is 3′-endo/anti, as for the other rGs in the stem.

CONCLUSION

We have shown here that vibrational spectrosopy, by its capability to elucidate local conformations of the nucleosides and nucleotides, permits the analysis of short-range conformational changes of RNA chains, such as UNCG tetraloops, which are the major folding sites of 16S RNA. Up to now, only NMR data of the UUCG and UACG tetraloop hairpins are available. Both series of data are consistent with similar rigid structures of these loops.

By a careful analysis of vibrational marker lines arising from the nucleosides included in the UCCG and UGCG hairpins, we have been able to confirm that all of the sugars involved in their stems and loops are of N-type except one, which is at the third position of the loop and is S-type. In the same way, all of the bases are oriented in the anti position vs sugar, except that located at the fourth position of the loop, which is syn oriented. We have validated by molecular modeling (results not reported) the possibility of forming UCCG and UGCG tetraloop hairpins with an N-type sugar included in their second nucleotide. The conformational angles of these theoretical structures are quite similar to those previously proposed for the UUCG (*7*) and UACG (*13*) tetraloops. The only exception is the δ angle of the second nucleotide, which follows the drastic change (S→N) of the sugar pucker. Of course, the new results reported in the present work concerning the particular behavior of the UCCG and UGCG tetraloops should be confirmed in the future by NMR spectra obtained from the same sequences.

It is also worth mentioning that the present work, as well as those on the UUCG and UACG tetraloops (*12*, *13*), constitutes the first successful attempt to use conformational marker lines, known from other structural studies of long-range regular DNA and RNA tracks, to study much shorter, nonrepetitive oligonucleotidic sequences.

REFERENCES

1. Tuerk, C., Gauss, P., Thermes, C., Groebe, D. R., Gayle, M., Guild, N., Stormo, G., Aubenton-Carafa, Y., Uhlenbeck, O. C., Tinoco, I., Jr., Brody, E. N., and Gold, L. (1988) *Proc. Natl. Acad. Sci. U.S.A. 85*, 1364−1368.
2. Uhlenbeck, O. C. (1990) *Nature 346*, 613−614.
3. Woese, C. R., Winker, S., and Gutell, R. R. (1990) *Proc. Natl. Acad. Sci. U.S.A. 87*, 8467−8471.
4. Wolters, J. (1992) *Nucleic Acids Res. 20*, 1843−1850.
5. Varani, G. (1995) *Annu. Rev. Biophys. Biomol. Struct. 24*, 379−404.
6. Sakata, T., Hiroaki, H., Oda, Y., Tanaka, T., Ikehara, M., and Uesugi, S. (1990) *Nucleic Acids Res. 18*, 3881−3839.
7. Cheong, C., Varani, G., and Tinoco, I., Jr. (1990) *Nature 346*, 680−681.
8. Varani, G., Cheong, C., and Tinoco, I., Jr. (1991) *Biochemistry 30*, 3280−3289.
9. Antao, V. P., Lai, S. Y., and Tinoco, I., Jr. (1991) *Nucleic Acids Res. 19*, 5901−5905.
10. Antao, V. P., and Tinoco, I., Jr. (1992) *Nucleic Acids Res. 20*, 819−824.
11. Molinaro, M., and Tinoco, I., Jr. (1995) *Nucleic Acids Res. 23*, 3056−3063.
12. Abdelkafi, M., Leulliot, N., Ghomi, M., Hervé du Penhoat, C., Namane, A., Gouyette, C., Huynh-Dinh, T., Baumruk, V., and Turpin, P.-Y. (1997) *J. Mol. Struct. 409*, 241−245.
13. Abdelkafi, M., Ghomi, M., Turpin, P.-Y., Baumruk, V., Hervé du Penhoat, C., Lampire, O., Bouchemal-Chibani, N., Goyer, P., Namane, A., Gouyette, C., Huynh-Dinh, T., and Bednarova, L. (1997) *J. Biomol. Struct. Dyn. 14*, 579−593.
14. Nowakowski, J., and Tinoco, I., Jr. (1996) *Biochemistry 35*, 2577−2585.
15. Allain, F. H. T., and Varani, G. (1995) *J. Mol. Biol. 250*, 333−353.
16. Bouchemal-Chibani, N., Lebrun, A., Herve du Penhoat, C., Ghomi, M., Laigle, L., Derouet, C., and Turpin, P.-Y. (1994) *J. Biomol. Struct. Dyn. 12*, 695−724.
17. Bouchemal-Chibani, N., Abdelkafi, M., Hervé du Penhoat, C., Ghomi, M., and Turpin, P.-Y. (1996) *Biopolymers 39*, 549−571.
18. Hanus, J., Kubelka, J., Baumruk, V., Praus, P., and Stepanek, J. (1995) *Proceedings of 10th Spectroscopic Conference with International Participation*, Czech Spectroscopic Society, Lanskroun.
19. Kanyo, J. E., Duhamel, J., and Lu, P. (1996) *Nucleic Acids Res. 24*, 4015−4022.
20. Small, E. W., and Peticolas, W. L. (1971)*Biopolymers 10*, 1377−1416.
21. Liquier, J., and Taillandier, E. (1996) in *Infrared Spectroscopy of Biomolecules* (Mantsch, H. H., and Chapman, D., Eds.) pp 131−158, Wiley-Liss, Inc., New York.
22. Small, E. W., Brown, K. J., and Peticolas, W. L. (1972) *Biopolymers 11*, 1209−1215.
23. Brown, K. G., Kiser, E. J., and Peticolas, W. L. (1972) *Biopolymers 11*, 1855−1869.
24. Prescott, B., Gamache, J., Livramento, J., and Thomas, G. J., Jr (1974) *Biopolymers 13*, 1821−1845.
25. Dohy, D., Ghomi, M., and Taillandier, E. (1989) *J. Biomol. Struct. Dyn. 6*, 741−754.
26. Liquier, J., Akhebat, A., Taillandier, E., Ceolin, F., Huynh Dinh, T., and Igolen, J. (1991) *Spectrochim. Acta 47a*, 177−186.

27. Letellier, R., Ghomi, M., and Taillandier, E. (1989) *J. Biomol. Struct. Dyn. 6*, 755−768.
28. Pohl, F. M., Ranade, A., and Stockburger, M. (1973) *Biochim. Biophys. Acta 335*, 85−92.
29. Thamann, T. J., Lord, R. C., Wang, A. H. J., and Rich, A. (1981) *Nucleic Acids Res. 20*, 5443−5447.
30. Nishimura, Y., Tsuboi, M., Uesugi, S., Ohkubo, M., and Ikehara, M. (1985) *Nucleic Acids Res. Symp. Ser. 16*, 25−28.
31. Trulson, M. O., Cruz, P., Puglisi, D., Tinoco, I., Jr., and Mathies, R. A. (1987) *Biochemistry 26*, 8624−8630.
32. Lafleur, B., Rice, J., and Thomas, G. J., Jr. (1972) *Biopolymers 11*, 2423−2437.

BI980011T